ADVANCED ELECTRONIC MATERIALS
www.advelectronicmat.de

Fully R2R-Printed Carbon-Nanotube-Based Limitless Length of Flexible Active-Matrix for Electrophoretic Display Application

Junfeng Sun, Ashish Sapkota, Hyejin Park, Prince Wesley, Younsu Jung, Bijendra Bishow Maskey, Yushin Kim, Yutaka Majima, Jianfu Ding, Jianying Ouyang, Chang Guo, Jacques Lefebvre, Zhao Li, Patrick R. L. Malenfant, Ali Javey,* and Gyoujin Cho**

A limitless-length flexible active-matrix implies that virtually any surface can be rendered into an interactive medium when laminated with electrophoretic or organic light-emitting diode sheets. However, performance, cost, and size limitations of current fabrication technologies and semiconducting materials, typically utilized in thin film transistor (TFT) active matrices (TFT-AMs), have hindered progress, thus preventing the realization of fully printed TFT-AMs on a plastic roll. A new high-purity semiconducting single-walled carbon nanotube (s-SWCNT) ink is prepared by first isolating 99.9% pure s-SWCNTs via conjugated polymer extraction, and then utilizing a ligand-exchange method to formulate a novel hydrophilic gravure-compatible semiconducting ink. Based on the s-SWCNT ink, a fully additive manufacturing process using roll-to-roll (R2R) gravure printing enables the fabrication of a flexible TFT-AM, overcoming performance, cost, and size limitations. TFT-AMs with 10 to 40 PPI resolution where average mobility of 0.23 ± 0.12 $cm^2 V^{-1} s^{-1}$, average on–off ratio of $10^{4.1}$, and threshold voltage variation of ±13% are attained. As a proof of concept, an inexpensive and flexible electrophoretic display is demonstrated by simply laminating an electrophoretic sheet onto the R2R gravure-printed s-SWCNT-based TFT-AM.

1. Introduction

To fully realize "limitless-length" flexible displays, a flexible thin film transistor active matrix (TFT-AM) should first be manufactured using a high-throughput and low-cost method to drive down the price and allow market accessibility.[1] Conceptually, large area flexible displays would transform any surface into an interactive medium that could conform to any underlying substrate. In such case, the flexible display would revolutionize our surroundings by driving the development of novel display form factors, through which leading to a human–machine interface revolution. To achieve this practically, TFT-AMs, a core technology for displays, should be manufactured without cost and size limitations.[1–3] The solution can be found in roll-to-roll (R2R) additive manufacturing, such as R2R gravure printing, which has been used as a low-cost manufacturing technology for newspapers, magazines, packaging, and wallpaper for over 100 years.[4] If this technology can be adopted to manufacture TFT-AMs for displays, a variety of flexible displays can be realized by simply laminating electrophoretic or organic light-emitting diode (OLED) sheets on R2R printed TFT-AMs (**Figure 1**a). To attain R2R-printed TFT-AMs with a comparable device yield and electrical performance to amorphous Si-based TFT-AMs, a rapidly curable (<5 s) semiconducting ink that yields a semiconducting thin film with an appropriate Fermi level to meet the work function of printed silver drain/source electrodes

Dr. J. Sun, Dr. H. Park, Dr. Y. Jung, B. B. Maskey, Prof. G. Cho
Department of Biophysics
Institute of Quantum Biophysics
Sungkyunkwan University
Suwon 16419, Korea
E-mail: gcho1004@skku.edu

A. Sapkota, Dr. J. Ding, Dr. J. Ouyang, Dr. C. Guo, Dr. J. Lefebvre, Dr. Z. Li, Dr. P. R. L. Malenfant
National Research Council Canada M-50
1200 Montreal Road, Ottawa, Ontario K1A 0R6, Canada
E-mail: Patrick.Malenfant@nrc-cnrc.gc.ca

The ORCID identification number(s) for the author(s) of this article can be found under https://doi.org/10.1002/aelm.201901431.

P. Wesley, Y. Kim
Department of Printed Electronics Engineering
Sunchon National University
Sunchon 57922, Korea

Prof. Y. Majima
Materials and Structure Laboratory
Tokyo Institute of Technology
Yokohama 226–8503, Japan

Prof. A. Javey
Electrical Engineering and Computer Sciences
University of California
Berkeley, CA 94720, USA
E-mail: ajavey@berkeley.edu

DOI: 10.1002/aelm.201901431

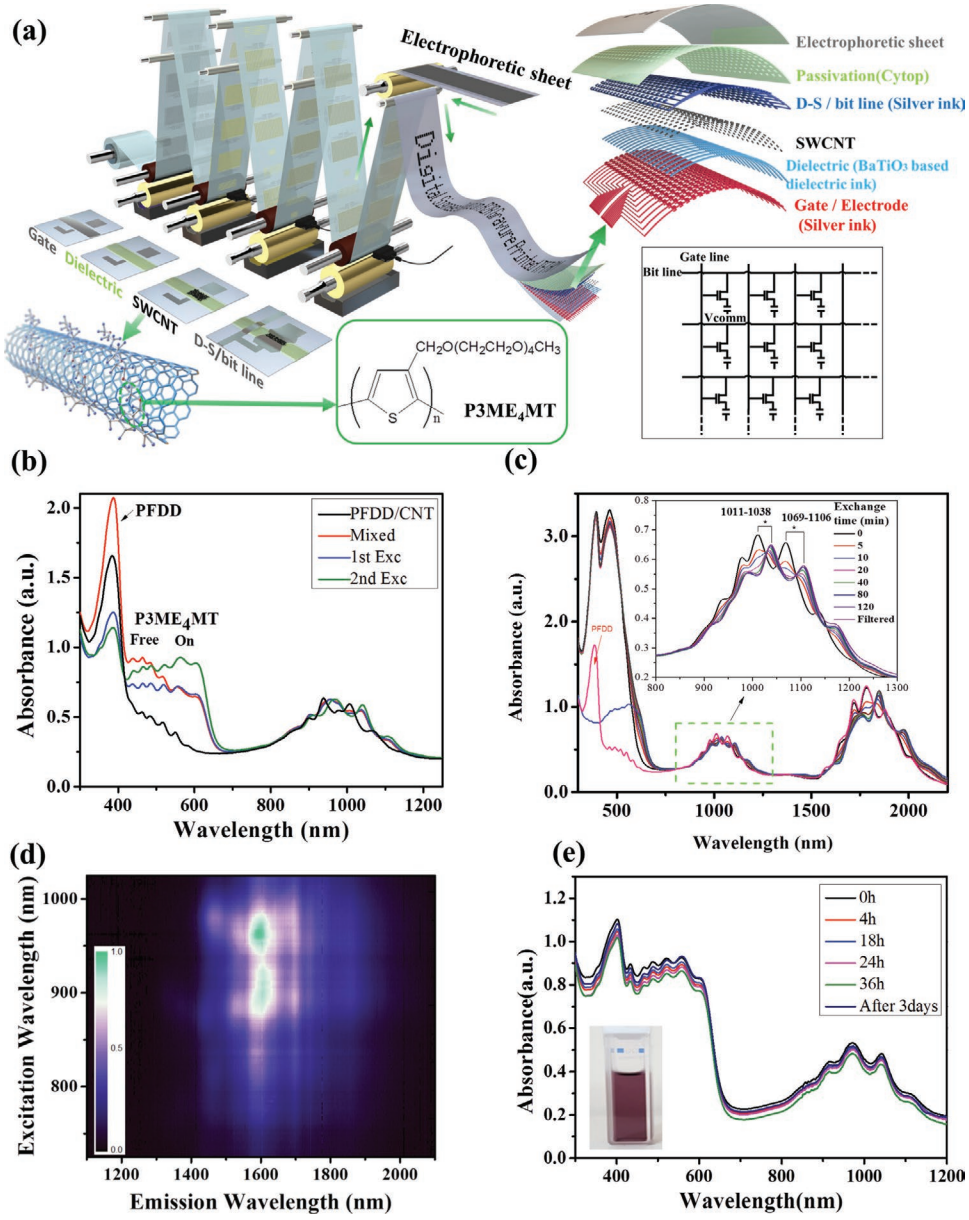

Figure 1. a) Concept image of fabricating digital signage by simply laminating OLED or electrophoretic sheets on R2R gravure printed TFT-active matrix based on pure s-SWCNT ink prepared via a new ligand ($P3ME_4MT$) exchange method (highlighted by a green box). b) UV–NIR absorption spectrum of sorted s-SWCNT sample (PFDD/CNT) at PFDD/CNT weight ratio of 1.25/1.00, and its mixture solution with equal amount of P3ME4MT(Mixed), and the re-dispersed solutions after the first and second polymer exchange (first Exc, and second Exc). c) The variation of the UV spectrum of the mixed solution during the polymer exchange process, where the original solution (PFDD) was prepared by dissolving 1.0 mg of PFDD/CNT composite with a PFDD/CNT weight ratio of 1.3/1 in 7 mL of toluene and bath sonicating for 30 min. d) PLE mapping image of s-SWCNT to show major (10, 9) chirality. e) UV–NIR absorption spectrum of formulated s-SWCNT ink to test the stability for 3 days (inset shows the formulated s-SWCNT ink).

and a minimum carrier mobility (>0.01 $cm^2\ V^{-1}\ s^{-1}$) is required.[5] Furthermore, low variation of threshold voltage (V_{th}) and high on–off current ratio of the printed TFT-AM are required to properly select the desired TFT pixels and avoid cross-talk between the pixels in the display.[6] Therefore, to properly operate a two-color electrophoretic display, the TFT-AM needs 0.01 $cm^2\ V^{-1}\ s^{-1}$ mobility, ±30% variation in the V_{th}, and 10^4 on–off current ratio while at least five times higher specifications may be needed to operate a full color display because of 5-bit addressing at each pixel required.[7,8] Although there are a few reports regarding flexible TFT-AM-based electrophoretic displays utilizing a hybrid fabrication method (printing, vacuum deposition, and photolithography),[9–11] no reports describe an all R2R-printed TFT-AM that meets the minimum requirements for mobility, on–off current ratio, and V_{th} variation, while also practically overcoming both manufacturing cost and size limitations. The reason being is that so far no semiconductor ink has been reliable and robust enough to be employed in a R2R gravure printing system.[12] Herein, high-purity semiconducting single-walled carbon nanotubes (s-SWCNTs) obtained via conjugated polymer extraction

were formulated into an ink via a ligand exchange method to meet critical requirements such as fast curing time (<5 sec),[12,13] low curing temperature (<150 °C), ambient stability, consistent ink transfer from the engraved cell, and proper wetting of the previously printed layer.[14,15] By employing the high-purity s-SWCNT-based ink, the R2R gravure-printed TFT-AM enabled both low-resolution (10 pixels per inch (PPI)) and high-resolution (40 PPI) TFT-AMs. Furthermore, a flexible digital display was demonstrated by utilizing a 20 × 20 TFT-AM with 10 PPI resolution cut out from the printed roll and simply laminated with an electrophoretic sheet to create a flexible electrophoretic display prototype that could easily be scaled for large-area signage (Figure 1a).

2. Results and Discussion

To obtain the desired high-purity s-SWCNTs in a compatible solvent for gravure printing, we first remove metallic SWCNTs using our previously reported extraction process with poly(9,9-didodecylfluorene) (PFDD) to obtain a semiconducting purity of 99.9%, followed by ligand exchange with a polythiophene derivative ($P3ME_4MT$) (highlighted in Figure 1a).[16,17] Excess $P3ME_4MT$ was mixed into the PFDD wrapped SWCNTs solution in toluene. The ligand exchange was assisted by bath sonication. During the ligand exchange process, we can confirm the packing of $P3ME_4MT$ onto the nanotube surface as its absorption peak at 464 nm shifts to longer wavelength at around 608 to form a shoulder in the ultraviolet (UV) spectrum (see Figure 1b).[18] This characteristic enables the estimation of the fraction of polymer on the nanotube surface as well as the free-polymer concentration in the solution. The S11 and S22 absorption peaks of the SWCNTs are also red-shifted significantly upon PFDD being replaced by $P3ME_4MT$ due to a more pronounced charge transfer interaction between the nanotubes and $P3ME_4MT$.[19] The stronger interaction between the nanotubes and polythiophenes compared to that with polyfluorenes facilitates the exchange, which can be tracked during the process by spectral changes. Therefore, to monitor this ligand exchange process, the solution was mixed with 5 mg of P3ME4MT in 1 mL of toluene. Its UV spectrum was recorded as 0 min, then the solution was bath sonicated at ≈40 °C for 5, 10, 20, 40, 80, and 120 min with UV spectra collected. Finally, the solution was filtered through a 0.2 μm filter to collect the nanotubes as the filtered sample, which was then re-dispersed in 8 mL of toluene to collect UV spectrum. The resulting UV–vis peak shifts as a function of time as shown in Figure 1c, which shows that the exchange takes ≈2 h to complete under bath sonication.

After filtration, a PFDD free sample is obtained with the PFDD peak completely removed from the UV spectrum of the re-dispersed solution. However, for the optimized SWCNT ink formulation, a fraction of PFDD (≈15% of the whole polymer weight) in the polymer/SWCNT composite was used. This was achieved by two ligand exchange cycles while the sonication time was limited to 30 min. This approach enables us to dial-in the desired s-SWCNT's dispersibility in polar solvents. In addition, the enrichment using PFDD ensured a high semiconductor purity, as confirmed by absorption and Raman spectroscopy.[20–22] Photoluminescence excitation (PLE) mapping confirms that the sorted s-SWCNTs mainly comprise nine chiralities, whereby a maximum of eight or nine chiralities appear to dominate the spectrum with the (10, 9) species being most abundant,[23] with a diameter of 1.30 nm (Figure 1d). $P3ME_4MT$ possesses hydrophilic ω-methoxy tetraethoxy methyl side chains, thus providing s-SWCNTs with good dispersibility in high-viscosity polar solvents with a good stability, suitable for gravure printing, such as butyl carbitol and 1-octanol with which the polythiophene derivative ($P3ME_4MT$) can interact, highlighted in Figure 1a. Optimized ink formulation (Section 4) provides adequate rheology for gravure printing and wetting onto printed dielectric layers to enable TFT device fabrication with suitable tube transfer without the need to rinse away $P3ME_4MT$. To the best of our knowledge, this approach has never been exploited to formulate a functional s-SWCNT ink for printing. The amphiphilic polymer design ($P3ME_4MT$) enables ink formulation directly into 1-octanol, while minimizing excipient use compared to aqueous dispersions, and without using any other surfactant or binder to optimize ink transfer (at a web transfer speed of 6 m min^{-1}). The ink, with a surface tension of 30 mN m^{-1} and a viscosity of 35 Cp, provided a good dispersion of s-SWCNTs (Figure 1e), which is critical since bundling of SWCNTs would have adverse effects on device performance. As formulated, this ink could be successfully transferred onto the printed dielectric layer at the aforementioned processing speed when the following conditions were met: 10° contact angle to the engraved gravure cell with 30 μm depth and 150 μm opening of the pyramidal structure for 10 PPI while 10 μm depth and 35 μm opening of the pyramidal structure for 40 PPI (Figure S1, Supporting Information). However, due to the different ink-transfer mechanism in printing high-resolution TFT-AMs with 40 PPI, the surface tension of the s-SWCNT ink was slightly altered by adding small amounts of toluene to the formulated s-SWCNT ink.

R2R gravure printing was performed following our previously reported method to fabricate a 20 × 20 TFT-AM with 10 PPI resolution (**Figure 2**a).[13] As shown in Figure 2b–d, the R2R gravure-printed TFT-AMs physically consists of TFTs with a gate electrode (width of 330 μm and thickness of 410 nm), pixel electrode (1320 μm × 1580 μm × 410 nm), a dielectric layer (width of 860 μm and thickness of 2.6 μm), a s-SWCNT layer (≈35 nanotubes per μm^2) and drain/source electrodes (width of 1320 μm and thickness of 420 nm) with a channel length of 80 μm. Remarkably, the physical dimensions are highly consistent along the whole length of the printed web (>10 m). Due to the consistency of the physical structures in the TFT-AMs, the device yield was approximately 98.5% when characterized by selecting 13 TFT pixels per TFT-AM every 2 m along the 10 m web (Figure 2e). The roll of printed devices was stored in the ambient and characterized under ambient conditions based on previously reported methods in which the effect of the quantum capacitance of the printed s-SWCNT network was negligible.[12,13] The V_{th} variation along 10 m of web was ±6% (Figure 2f), with an average mobility of 0.03 ± 0.004 cm^2 V^{-1} s^{-1} (Figure 2g) and average on–off current ratio of $10^{4.3 \pm 0.1}$ (Figure 2h). Furthermore, an acceptable range of hysteresis (0.5–3.5 V) along the 10 m length on the printed web was observed (Figure 2i). Furthermore, the electrical parameters (such as the mobility, on–off ratio, and V_{th})

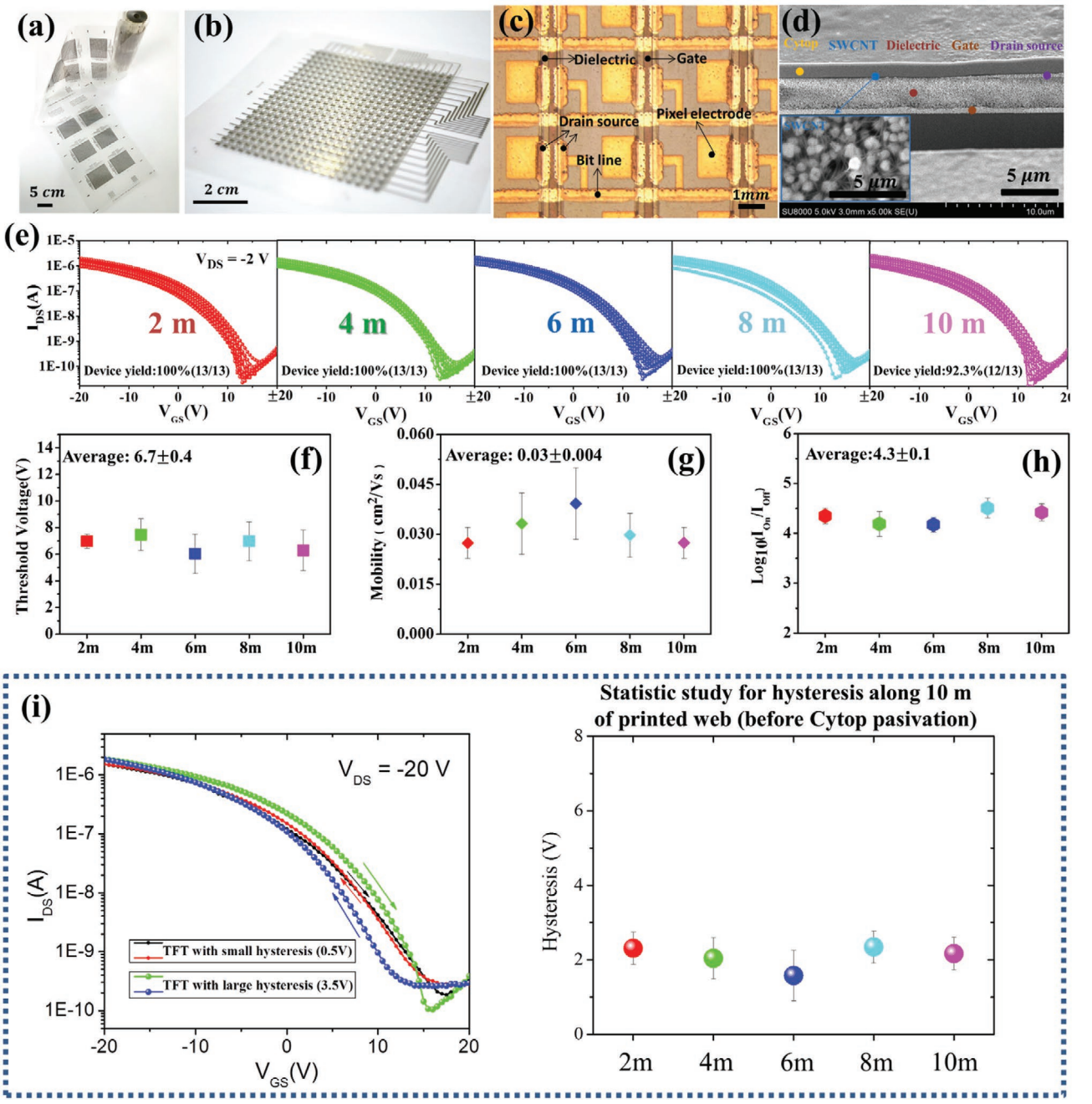

Figure 2. a) Roll of R2R gravure printed TFT-active matrix with 10 PPI resolutions and b) one selected TFT-active matrix. c) Optical images of nine pixels and d) a cross-sectional FIB-SEM image with the inset of printed s-SWCNTs on printed dielectric layer. e) Transfer characteristics of TFTs attained from selected 13 TFT pixels per TFT-AM every 2 m along the 10 m web. f) The statistical data of extracted threshold voltage (V_{th}), g) mobility, and h) on–off current ratio. i) Typical transfer characteristics of TFTs with the smallest and largest hysteresis and statistical study of the hysteresis for 13 TFTs without passivation per every 2 m along 10 m length of the web.

of 20 × 20 TFT-active matrix were characterized under bending state with a diameter of 20 mm (Figure S2a, Supporting Information). The attained electrical parameters were all showed negligible variations comparing with those values to the resting state (Figure S2b, Supporting Information). Based on the electrical characteristics of the TFT-AM collected every 2 m along 10 m of web, the high-purity s-SWCNT-based ink can be printed homogeneously without any coffee ring effect (Figure S3, Supporting Information) and provides a reliable and practical solution to manufacture a limitless-length of TFT-AMs. To further prove the scalability of the R2R gravure system in terms of both size and resolution, a TFT-AM measuring 2.4 × 3.15 in.^{2} with 40 PPI resolution was printed under the same R2R conditions. However, no electrical characteristics were observed due to insufficient transfer of s-SWCNT ink, even with well-printed layers for gate electrodes, dielectric layers, and drain/source

electrodes (Figure S4, Supporting Information). In fact, the transfer of lower viscosity ink is more sensitive to variations in the cell structure than that of higher viscosity inks for printing gate, dielectric, and drain-source electrodes. Based on a simulation of s-SWCNT ink transfer, the transfer of s-SWCNT-based ink was not as effective as observed in printing 10 PPI TFT-AM (Figure S5a, Supporting Information) due to the high surface tension of the ink in combination with the shrunken gravure cell used to print the 40 PPI TFT-AM (Figure S5b, Supporting Information). Adding small amounts of toluene to the s-SWCNT ink reduced the surface tension, allowing effective transfer from the gravure cell (Figure S5c, Supporting Information). Modifying the surface tension gave the s-SWCNT-based ink a similar viscosity to 1-octanol-based ink, 34 Cp, but with a lower surface tension of 28 mN m^{-1} (Figure S6, Supporting Information). Using this ink, a 76 × 109 TFT-AM with 40 PPI was successfully R2R gravure printed, with a device yield of 95%. The yield was determined by measuring 80 randomly selected TFT pixels per TFT-AM every 2 m along the 10 m web (Figure S7, Supporting Information). The average mobility was 0.41 ± 0.12 cm^2 V^{-1}, with an average ± 29% variation in V_{th} and average on–off current of $10^{4.2}$. All device characteristics were similar to those of the 10 PPI TFT-AMs, except for the one-order-higher mobility. The higher mobility results from the increased ink-transfer rate using the shrunken gravure cell and shorter channel length.[24] Based on the 10 PPI and 40 PPI TFT-AMs results, a 40 PPI TFT-AM with a size of 2.75 × limitless in.^{2} could be designed by simply connecting the beginning and end electrodes of the row-lines in the TFT-AM on the gravure cylinder (Figure S8, Supporting Information). With one rotation of this gravure cylinder, a 16.1 inch-long TFT-AM with 40 PPI (**Figure 3**a) was fabricated with 92% device yield (Figure 3b). When rotated 100 times, a 1610 inch-long TFT-AM with 40 PPI can be printed. As such, a R2R-printed, 40 PPI TFT-AM produced from five rotations of the gravure cylinder, giving a size of 2.4 × 80.3 in.^{2}, was selected for characterization, and the measured average electrical characteristics, that is, the mobility (0.23 ± 0.12 cm^2 V^{-1} s^{-1}), average on–off current ratio ($10^{4.1}$), and average V_{th} variation (± 13%) (Figure 3c–e) were comparable to those of the 76 × 109 TFT-AM with 40 PPI. From these results, we conclude that the high-purity s-SWCNT-based R2R gravure system is indeed scalable for the fabrication of large area flexible TFT-AMs with low cost and consistent electrical properties. Specifically, a 60 m long, wall-sized display with a resolution of 40 PPI could be manufactured within 15 min via R2R lamination of an electrophoretic sheets onto a R2R-printed TFT-AM.

To demonstrate R2R gravure-printed TFT-AM-based signage, we selected a 20 × 20 TFT-AM with 10 PPI resolution due to the ease of construction of the driving IC. Before lamination

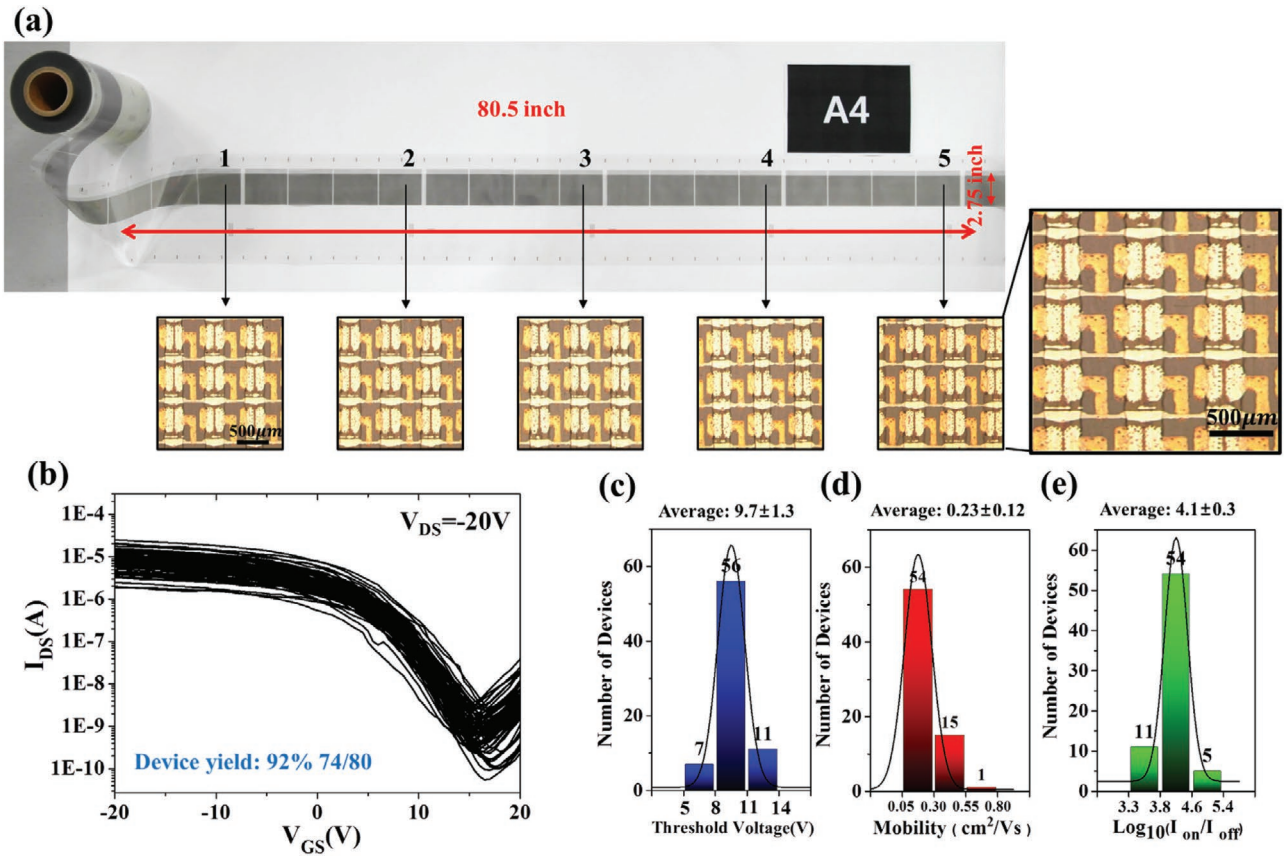

Figure 3. a) Optical image of R2R gravure printed limitless-length 40 PPI TFT-active matrix. b) Attained transfer characteristics by randomly measured 80 TFTs from randomly selected 16.1 inch length web. c) Statistical data of extracted threshold voltage (V_{th}), d) mobility, and e) on–off current ratio attained from randomly measured 80 TFTs.

of the electrophoretic sheet onto the 10 PPI TFT-AM, 400 TFT pixels were characterized to understand the behavior of each TFT pixel in the TFT-AM. The results for 400 TFTs randomly selected among different TFT-AMs were almost statistically identical along 10 m of web length (Figure S9, Supporting Information). However, during characterization of all 400 TFTs in a TFT-AM under ambient condition, a large variation in V_{th} was observed (Figure S9a, Supporting Information) due to exposure to ambient conditions. The attained variation in V_{th} from 400 TFTs was ±24% (Figure S9b, Supporting Information), with an average mobility of 0.03 ± 0.007 $cm^2\ V^{-1}\ s^{-1}$ (Figure S9c, Supporting Information) and average on-off current ratio of $10^{3.7\ \pm\ 0.4}$ (Figure S9d, Supporting Information). Because a narrow variation in V_{th} is necessary to properly operate the electrophoretic display, the large variation in V_{th} due to humidity must be mitigated through passivation. However, because the V_{th} of s-SWCNT-TFT is very sensitive to material contact, the shift in V_{th} must be minimized upon passivation. Among previously reported materials used to passivate SWCNT-based TFTs, epoxy,[25] poly(methylmethacrylate),[26] Cytop, and poly(vinylphenol) were explored,[27,28] and spin-coated Cytop showed the best passivation effect (Figure S10, Supporting Information). Based on our experience in passivating SWCNT-based TFTs, hydrophobic polymers without any electron donating groups such as hydroxyl, amine, and carbonyl groups work well because s-SWCNTs are very vulnerable to moisture and molecules with polar groups.

After Cytop passivation (**Figure 4**a), the R2R gravure-printed TFT-AM (400 TFTs) was characterized again (Figure 4b–e). The V_{th} was stable with a variation of ±5.6% (Figure 4c) and maintained a similar mobility (0.02 ± 0.005 $cm^2\ V^{-1}\ s^{-1}$) (Figure 4d) and on–off ratio ($10^{3.5\ \pm\ 0.6}$) (Figure 4e) to the non-passivated devices (Figure S9c,d, Supporting Information). The variation in V_{th} garnered from the 400 TFTs is the best result among currently reported fully printed TFTs and can operate electrophoretic display pixels.[13,29] Furthermore, the average on–off current ratio generated from the TFTs was enough to switch each pixel. A single transistor can switch a pixel with dimensions of 1320 × 1580 μm^2 because each transistor provides at least 600 nA of "on" current when the gate voltage is −20 V and the source voltage is −5 V. In addition, to avoid cross-talk with neighboring pixels, a single TFT in a series of pixels of the TFT-AM should not generate more than ≈10 nA of "off" current when the TFTs are set to the "off" status at a gate voltage of +20 V (Figure S11, Supporting Information). Based on the individual TFT characteristics, applying a voltage to a row (gate) (−20 V) and a column (source) (−5 V) of electrodes while maintaining a steady voltage as a common voltage (−15 V) turns on the pixel and provides a black color. To turn off the pixel (white color), the column was kept at −20 V and the row at −20 V while maintaining a steady voltage of −15 V. Depending on the applied potential difference on the electrophoretic sheet, the best contrast of black color was observed when the potential difference was −10 V (Table S1, Supporting Information). To fully control 20 × 20 pixels, we employed a driving IC (Figure S12, Supporting Information) to operate the electrophoretic display, with a switching speed of 0.3 Hz to ensure each pixel operated (see Video S1, Supporting Information). It should be noted that the functional switching speed can be increased to 10 Hz with this driving integrated circuit (IC) system; the switching speed is limited by the electrophoretic sheet. By changing the electrophoretic sheet to one manufactured by e-ink, the on–off switching speed can reach more than 10 Hz (Video S1, Supporting Information). Based on these operating conditions, a R2R gravure printed TFT-AM was utilized for the first time to demonstrate the proper operation of an 0.4 mm thick electrophoretic display showing the words "P," "E," and "RIC" (Figure 4f and Video S2, Supporting Information). However, even with a TFT-AM device yield higher than 95% before the lamination of electrophoretic sheet, dead-pixels were observed in the laminated display (Figure 4f). To elucidate the root cause of the dead pixels generated during the lamination process, we selected the printed TFT-active matrix with a device yield of 99% in which only 3 TFTs were short and one TFT was open, and the letter "R" with 44 pixels was displayed after extracting all 400 TFTs' transfer characteristics and leakage currents as shown in Extra Analysis and Figure S13, Supporting Information. Through retrieving and analyzing both for the leakage currents and off current for the 44 controllable "live-pixels" and 16 uncontrollable "dead-pixels" (Figures S14 and S15, Supporting Information), these 16 pixels showed high leakage at the junction of each pixel as shown in Figure S16, Supporting Information. The leakage levels at those pixels were a lot higher than the controllable pixels. This is understandable since the junction areas, having three printed layers, will have relatively higher height and narrow area than any other area in the TFT-AM resulting in a thinner insulating layer. We observed that the controllable live-pixels in the sample had leakage current less than about 30 nA, whereas the uncontrollable dead-pixels had leakage current levels greater than 30 nA at the junction of the electrodes. Hence, the higher leakage current levels at the crossing junction is the root cause for most of the dead-pixels despite the TFT fabrication yield being over 95%. To overcome the types of dead pixels generated during the lamination process, we simply anticipate needing to increase the junction area or reduce the thickness of the bottom electrodes. As we explore different applications, optimizations will be made to the TFT-AM to accommodate downstream processes such as the lamination of active display layers.

3. Conclusion

In summary, a high-purity semiconducting SWCNT ink was obtained by carefully tailoring the surface properties of the nanotubes by replacing the wrapping polymer (PFDD) with an amphiphilic polythiophene derivative ($P3ME_4MT$), which enabled the formulation of a gravure ink in 1-octanol, a benign solvent, that meets the rheological properties required for the R2R gravure system. Based on this novel ink, TFT-AMs from low resolution (10 PPI) to high resolution (40 PPI) can be fully R2R printed at a printing speed of 6 m min^{-1}, overcoming performance, cost, and size limitations plaguing conventional materials and approaches. The fully R2R printed TFT-AMs with 10 PPI resolution showed a 96.5% device yield, an average mobility of 0.02 ± 0.005 $cm^2\ V^{-1}\ s^{-1}$, average on–off current ratio of $10^{3.5\ \pm\ 0.6}$, with a V_{th} variation of ±5.6% after Cytop passivation. A TFT-AM with 40 PPI

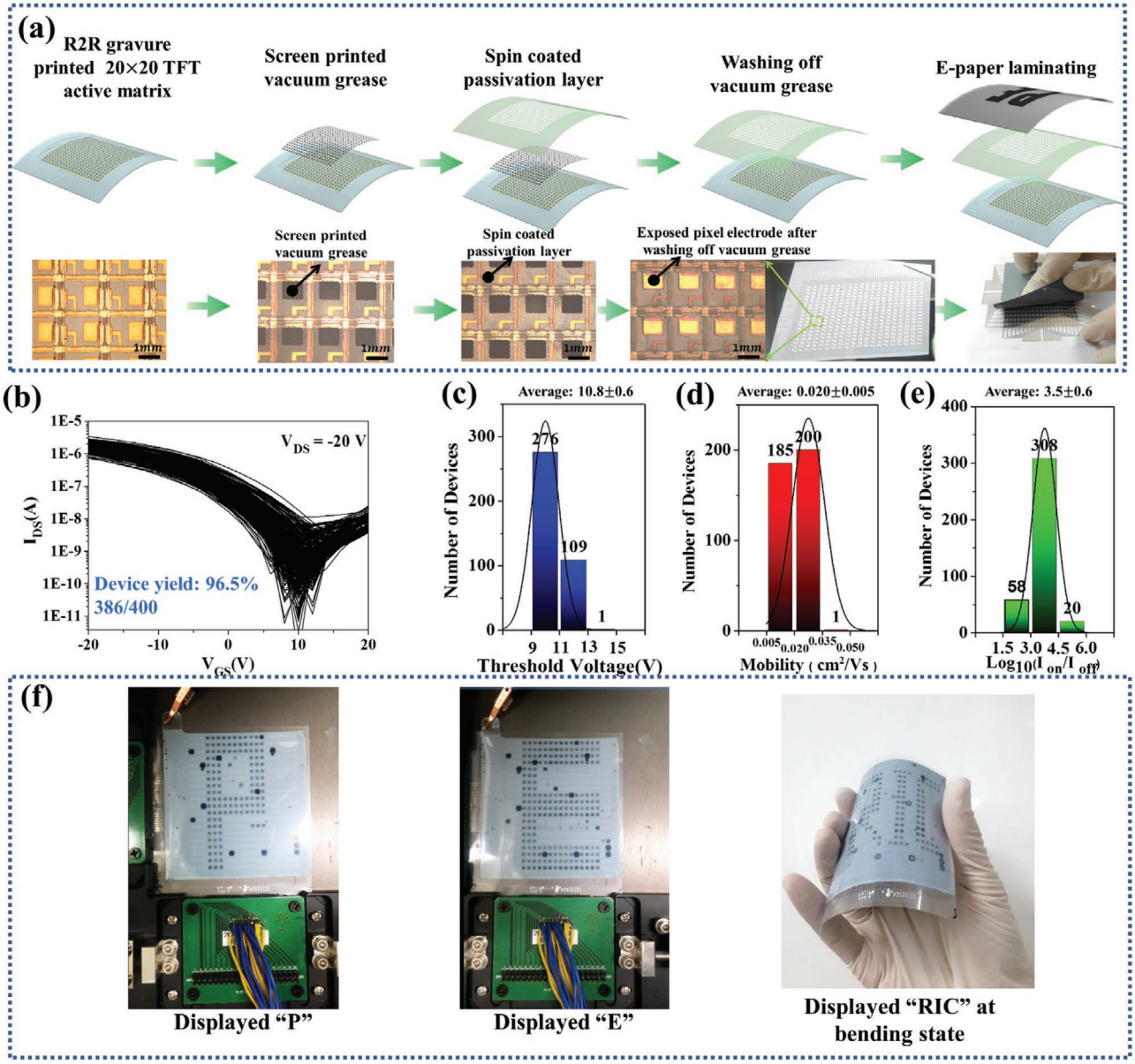

Figure 4. a) R2R gravure printed 20 × 20 TFT active matrix based electrophoretic signage fabrication process: the selected TFT-active matrix was spun coated with Cytop after masking pixel electrodes by vacuum grease and then, washed off the vacuum grease to reveal the electrodes again to contact the bottom electrodes of the electrophoretic sheet by laminating the sheet. b) Characteristics of TFTs attained from 400 TFTs in a 20 × 20 printed TFT-AM after passivation with Cytop. c) The statistical data of extracted threshold voltage (V_{th}), d) mobility, e) on–off current ratio. f) The resulting e-paper was operated by a custom made driving IC system to show words such as "P," "E," and "RIC."

resolution yielded a 2.75 × 80.3 in.^{2} TFT array along 10 m of web, with a consistent device yield (92%), an average mobility of 0.23 ± 0.12 cm^2 V^{-1} s^{-1}, average on–off current ratio of $10^{4.1}$, and a V_{th} variation of ±13%. Because this R2R gravure system demonstrated practical device yield (>92%) with consistent electrical properties along the entire length of the 10 m PET web with no limitation in the resolution up to 40 PPI, the flexible and roll-able TFT-AM could be easily scaled with low cost. Furthermore, the insights obtained herein suggest that the R2R gravure-printed TFT-AM can be extended to operate OLED displays by improving the mobility of TFTs up to 5 cm^2 V^{-1} s^{-1}, while keeping the presently attained V_{th} variation (±5%).[28,30] With regards to improving the yield of the process to 100%, the PET substrate should not be contaminated by oils or plasticizer and be free from all precipitated or adsorbed nano-particles or other contaminants. To achieve this, a clean room with a higher class (<1000) and particle-free PET roll should be employed to avoid open-circuit device failures in the R2R printed TFT-AM due to insufficient SWCNT-ink transfer (active layer). By utilizing a clean room with a higher class, the reported R2R gravure system can be utilized to print a TFT active matrix with maximum 150 PPI resolution (Figure S17, Supporting Information). The results reported above are the first steps in realizing a printed display

based on limitless-web length that can be directly utilized in current packaging and large-area flexible signage technology.

4. Experimental Section

Materials: The silver nanoparticle-based gel-type ink used to print gates, contact electrodes, and drain/source electrodes was purchased from PARU (PG-007), and its viscosity was adjusted to 1000 Cp to print the gate and contact electrodes, while a viscosity of 1200 Cp was used to print the drain/source electrodes. $BaTiO_3$ nanoparticle-based dielectric ink was also purchased from PARU (PD-100) and used without any further dilution. s-SWCNTs were prepared using a reported PFDD extraction process using plasma SWCNTs and a PFDD/CNT ratio of 1.25/1.00. Then, 300 mg of this sample was added with 300 mg of $P3ME_4MT$ in 1000 mL of toluene. The mixture was bath sonicated for 30 min to completely disperse the SWCNTs and form a homogeneous solution, which was then filtered through a Teflon membrane with a pore size of 0.2 µm (Sartorius Stedim Biotech GmbH) to collect the SWCNTs. The obtained film was soaked in toluene to remove free polymer. This exchange step was repeated once more using 750 mg of PME_4MT to obtain the final sample, which was dried before formulation as a semiconducting ink using 1-octanol (Junsei Chemical Co., Ltd., Japan). The sorted SWCNTs (15 mg) were dispersed in 1-octanol (30 mL) using probe sonication for 3 h. The resulting ink provided a stable dispersion of s-SWCNTs, and its stability was characterized by UV–NIR spectroscopy (JASCO V-670). Furthermore, its rheological characteristics were studied using a HAAKE MARS modular advanced rheometer system at 25 °C.

TFT-AMs Fabrication Using R2R Gravure Printing: In general, the R2R gravure printing method was the same as previously reported methods, where a temperature of 25 °C and humidity of 35% were maintained in a clean room (10000 class), and the summary of printing parameters are shown in Table S2, Supporting Information.[12] First, gate electrodes and contact electrodes were printed at a speed of 6 m min^{-1} using silver nanoparticle-based ink. Then, the dielectric layers were printed at the same speed using $BaTiO_3$ nanoparticle-based ink. The resulting printed PET web was rewound to print the s-SWCNTs at the same speed. After printing the s-SWCNTs, the web was rewound again to print drain/source electrodes and wires at the same speed. The resulting s-SWCNT-based TFT-AMs with resolutions of 10 PPI and 40 PPI were characterized by selecting one TFT-AM every 2 m along 10 m of PET web. To demonstrate the limitless length of 40 PPI TFT-AM fabrication, 80.3 inch of TFT-AM, printed by five rotations of the gravure cylinder, was selected along the length of the 10 m web to characterize the device yield with electrical properties.

Laminating Electrophoretic Sheet on the R2R Gravure-Printed TFT-Ams: For the operational demonstration of e-paper using the R2R gravure-printed TFT-AMs, the electrophoretic sheet was laminated on the TFT-AM via exposed contact electrodes in the TFT-AM, where TFTs were passivated by first screen printing vacuum grease only on the contact electrodes by semi-auto screen printer (SM-S320 manufactured by SUNMECHANIX Co., Korea). Cytop (Asahi Glass Co., Japan) was then spin coated twice with 650 rpm for 0.5 min under ambient condition using the commercially available Cytop solution. After spin coating, the printed vacuum grease was washed away by hexane to selectively expose the contact electrodes to contact the bottom electrodes of the electrophoretic sheet (Figure 4a).

TFT Characterization: The transfer, output, and leakage characteristics of TFTs in the active matrix were measured using a KEITHLEY 4200 Semiconductor Characterization System (USA) with an ambient probe station (MS TECH(MST-4000A)). All attained data were analyzed using a custom Origin script to obtain the mobility, threshold voltage, and on–off current ratio.

Electrophoretic Display Demonstration: The e-paper demonstration was carried out using a custom-made controller that employed the row-to-row scanning (gate line) method. The microcontroller (ATmega2560) used in this driving IC could only supply voltage in the range 0–5 V. Therefore, to drive the R2R gravure-printed TFT-AM-based e-paper, a higher voltage (–20 to +20 V) was needed. To provide enough voltage, a level shifter circuit was designed by using Opamp (LT1491) to convert the low digital output voltage (0–5 V) to higher voltage (–20 to +20 V). To show a particular image on the e-paper, the e-paper was first turned to the white (clear) state (V_{comm} = +20 V; V_g = –20 V; V_s = –20 V). After V_{comm} was set to –15 V, the gate lines were scanned one by one (the voltage of the gate scan lines was –20 V, while the other scan lines had a voltage of +20 V). The source lines were set to the desired value (ON: V_s of –5 V and OFF: V_s of –20 V) to control the e-paper pixels. To control the contrast of the e-paper, the V_{comm} potential was increased from –10 to –15 V as the pixels became darker due to the increase in the potential difference between the top and bottom electrodes of the electrophoretic sheet. The scanning rate of the gate lines also affected the contrast of the display.

Supporting Information

Supporting Information is available from the Wiley Online Library or from the author.

Acknowledgements

The authors thank the Institute for Information & Communications Technology Promotion (IITP) grant funded by the Korea government of Ministry of Science and ICT (MSIT) (No. 2018-0-00389) and the Global Leading Technology Program of the Office of Strategic R&D Planning (OSP), funded by the Ministry of Commerce, Industry and Energy, Republic of Korea (10042537, Printed Electronics Total Solution Development).

Conflict of Interest

The authors declare no conflict of interest.

Keywords

additive manufacturing, carbon nanotubes, e-paper, flexible TFTs, active matrices, roll-to-roll gravure

Received: December 24, 2019
Revised: February 18, 2020
Published online: March 5, 2020

[1] J. C. Goh, H. J. Chung, J. Jang, C. H. Han, *IEEE Electron Devices Lett.* **2002**, *23*, 544.
[2] P. Chen, Y. Fu, R. Aminirad, C. Wang, J. Zhang, K. Wang, K. Galatsis, C. Zhou, *Nano Lett.* **2011**, *11*, 5301.
[3] T. Shirasaki, T. Ozaki, K. Sato, M. Takei, T. Toyama, S. Shimoda, T. Tano, *SID Symp. Dig. Tech. Pap.* **2004**, *35*, 1516.
[4] O. M. Lilien, *History of Industrial Gravure Printing up to 1920*, Lund Humphries Publishers, London **1972**.
[5] T. Y. Kim, M. Amani, G. H. Ahn, Y. Song, A. Javey, S. Chung, T. Lee, *ACS Nano* **2016**, *10*, 2819.
[6] X. Cao, C. Lau, Y. Liu, F. Wu, H. Gui, Q. Liu, H. Wan, C. Zhou, *ACS Nano* **2016**, *10*, 9816.
[7] G. Gelinck, P. Heremans, K. Nomoto, T. D. Anthopoulos, *Adv. Mater.* **2010**, *22*, 3778.

[8] S. J. Telfer, M. D. McCreary, *SID Symp. Dig. Tech. Pap.* **2016**, *47*, 574.
[9] J. A. Rogers, Z. Bao, K. Baldwin, A. Dodabalapur, B. Crone, V. R. Raju, V. Kuck, H. Katz, K. Amundson, J. Ewing, P. Drzaic, *Proc. Natl. Acad. Sci. U. S. A.* **2001**, *98*, 4835.
[10] G. H. Gelinck, H. E. A. Huitema, E. van Veenendaal, E. Cantatore, L. Schrijnemakers, J. B. P. H. van der Putten, T. C. T. Geuns, M. Beenhakkers, J. B. Giesbers, B.-H. Huisman, E. J. Meijer, E. M. Benito, F. J. Touwslager, A. W. Marsman, B. J. E. van Rens, D. M. de Leeuw, *Nat. Mater.* **2004**, *3*, 106.
[11] K. Suzuki, K. Yutani, M. Nakashima, A. Onodera, S. Mizukami, M. Kato, T. Tano, H. Tomono, M. Yanagisawa, K. Kameyama, *Proc. IDW* **2009**, *09*, 1581.
[12] J. Sun, H. P , Y. Jung, G. Rajbhandari, B. B. Maskey, A. Sapkota, Y. Azuma, Y. Majima, G. Cho, *ACS Omega* **2017**, *2*, 5766.
[13] W. Lee, H. Koo, J. Sun, J. Noh, K.-S. Kwon, C. Yeom, Y. Choi, K. Chen, A. Javey, G. Cho, *Sci. Rep.* **2015**, *5*, 17707.
[14] J. Noh, M. Jung, Y. Jung, C. Yeom, M. Pyo, G. Cho, *Proc. IEEE* **2015**, *103*, 554.
[15] P. Kopola, M. Tuomikoski, R. Suhonen, *Thin Solid Films* **2009**,*517*, 5757.
[16] S. D. Stranks, A. M. R. Baker, J. A. Alexander-Webber, B. Dirks, R. J. Nicholas, *Small* **2013**, *9*, 2245.
[17] S. D. Stranks, S. N. Habisreutinger, B. Dirks, R. J. Nicholas, *Adv. Mater.* **2013**, *25*, 4365.
[18] S. D. Stranks, C. Weisspfennig, P. Parkinson, M. B. Johnston, L. M. Herz, R. J. Nicholas, *Nano Lett.* **2011**, *11*, 66.
[19] T. Schuettfort, H. J. Snaith, A. Nish, R. J. Nicholas, *Nanotechnology* **2010**, *21*, 025201.
[20] J. Ding, Z. Li, J. Lefebvre, F. Cheng, G. Dubey, S. Zou, P. Finnie, A. Hrdina, L. Scoles, G. P. Lopinski, C. T. Kingston, B. Simard, P. R. L. Malenfant, *Nanoscale* **2014**, *6*, 2328.
[21] J. Ding, Z. Li, J. Lefebvre, F. Cheng, J. L. Dunford, P. R. L. Malenfant, J. Humes, J. Kroeger, *Nanoscale* **2015**, *7*, 15741.
[22] Z. Li, J. Ding, P. Finnie, J. Lefebvre, F. Cheng, C. T. Kingston, P. R. L. Malenfant, *Nano Res.* **2015**, *8*, 2179.
[23] S. M. Bachilo, M. S. Strano, C. Kittrell, R. H. Hauge, R. E. Smalley, R. B. Weisman, *Science* **2002**, *298*, 2361.
[24] H. Sirringhaus, T. Kawase, R. H. Friend, T. Shimoda, M. Inbasekaran, W. Wu, E. P. Woo, *Science* **2000**,*290*, 2123.
[25] D. Kim, Y. Jung, J. Sun, C. Yeom, H. Park, D. Jung, Y. Ju, K. Chen, A. Javey, G. Cho, *Nanoscale* **2016**, *8*,19876.
[26] Y. Yang, Z. Wang, Z. Xu, K. Wu, X. Yu, X. Chen, Y. Meng, H. Li, S. Qiu, H. Jin, L. Li, Q. Li, *ACS Appl. Mater. Interfaces* **2017**, *9*, 14292.
[27] T. J. Ha, D. Kiriya, K. Chen, A. Javey, *ACS Appl. Mater. Interfaces* **2014**, *6*, 8441.
[28] C. M. Homenick, R. James, G. P. Lopinski, J. Dunford, J. Sun, H. Park, Y. Jung, G. Cho, P. R. L. Malenfant, *ACS Appl. Mater. Interfaces* **2016**, *8*, 27900.
[29] C. Yeom, K. Chen, D. Kiriya, Z. Yu, G. Cho, A. Javey, *Adv. Mater.* **2015**, *27*, 1561.
[30] J. Lefebvre, J. Ding, Z. Li, P. Finnie, G. Lopinski, P. R. L. Malenfant, *Acc. Chem. Res.* **2017**, *50*, 2479.

